

Vision Aided Channel Prediction for Vehicular Communications: A Case Study of Received Power Prediction Using RGB Images

Xuejian Zhang, *Student Member, IEEE*, Ruisi He, *Senior Member, IEEE*, Mi Yang, *Member, IEEE*, Zhengyu Zhang, *Student Member, IEEE*, Ziyi Qi, Bo Ai, *Fellow, IEEE*

Abstract—The communication scenarios and channel characteristics of 6G will be more complex and difficult to characterize. Conventional methods for channel prediction face challenges in achieving an optimal balance between accuracy, practicality, and generalizability. Additionally, they often fail to effectively leverage environmental features. Within the framework of integration communication and artificial intelligence as a pivotal development vision for 6G, it is imperative to achieve intelligent prediction of channel characteristics. Vision-aided methods have been employed in various wireless communication tasks, excluding channel prediction, and have demonstrated enhanced efficiency and performance. In this paper, we propose a vision-aided two-stage model for channel prediction in millimeter wave vehicular communication scenarios, realizing accurate received power prediction utilizing solely RGB images. Firstly, we obtain original images of propagation environment through an RGB camera. Secondly, three typical computer vision methods including object detection, instance segmentation and binary mask are employed for environmental information extraction from original images in stage 1, and prediction of received power based on processed images is implemented in stage 2. Pre-trained YOLOv8 and ResNets are used in stages 1 and 2, respectively, and fine-tuned on datasets. Finally, we conduct five experiments to evaluate the performance of proposed model, demonstrating its feasibility, accuracy and generalization capabilities. The model proposed in this paper offers novel solutions for achieving intelligent channel prediction in vehicular communications.

Index Terms—Channel prediction, vehicular communications, deep learning, vision information.

I. INTRODUCTION

THE future 6G vision articulated by ITU-R highlights the integration of communication and artificial intelligence (AI) as a critical emerging technology trend [2], [3]. Consequently, the development of more efficient and reliable wireless communication systems leveraging AI technology has garnered significant attention in the research community

[4]. At the same time, communication scenarios of 6G are increasingly complex, featuring three-dimensional communication across air-space-ground, higher frequency bands such as millimeter waves and terahertz, wider bandwidths, and massive multiple-input multiple-output (MIMO) systems [5]. These aspects represent both new development trends and challenges [6]. They heavily utilize valuable spatio-temporal-frequency resources, imposing additional communication costs and greater computational resource consumption on wireless communication systems [7], and are not conducive to establishment of wireless communication systems with efficient resource utilization for 6G.

Recently, with explosive advances in computer vision (CV) technology and growing interest in using AI to solve key wireless communication challenges [8]–[10], large amounts of out-of-band information and data, such as visual sensing data, have been introduced into wireless communication systems, since their acquisition does not occupy other frequency resources, it is beneficial to reduce communication overhead and improve spectrum efficiency. What's more, with gradual development of intelligent services such as intelligent transportation and autonomous driving, vehicle and infrastructure will be installed with rich variety of sensors such as radar, LiDAR, depth/RGB cameras, which will make acquisition of visual data easier [11]. Visual data obtained can be used to assist various vehicular communications, such as vehicle-to-vehicle (V2V) and vehicle-to-infrastructure (V2I) communications, i.e., enabling vision-aided wireless communications [12]. It has been shown to significantly enhance wireless communication reliability without sacrificing spectral efficiency [13], [14].

Channel prediction is one of potential typical applications that can be aided by visual information [15]. Accurate channel prediction is the foundation of intelligent vehicular communications [16], [17]. Moreover, there is actually a natural match between channel and visual data because wireless channel is determined by propagation environment which can be recorded in the form of visual data. Based on vision information, sizes, shapes and positions of scatterers can be reflected, effectively indicating wireless propagation features, and typical channel characteristics, including received power, path loss, etc., can be inferred. Further, this method can be used to provide valuable guidance for design and deployment of intelligent vehicular communication systems. For example, it can assist in determining the optimal number and spacing of base stations, as well as dynamically adjusting base station power in real

Part of this paper has been presented in the IEEE International Symposium on Antennas and Propagation and ITNC-USNC-URSI Radio Science Meeting (IEEE AP-S-2024) [1].

X. Zhang, R. He, Z. Zhang, Z. Qi and B. Ai are with the School of Electronics and Information Engineering and the Frontiers Science Center for Smart High-speed Railway System, Beijing Jiaotong University, Beijing 100044, China (email: 23115029@bjtu.edu.cn; ruisi.he@bjtu.edu.cn; 21111040@bjtu.edu.cn; 22115006@bjtu.edu.cn; boai@bjtu.edu.cn).

M. Yang is with the School of Electronics and Information Engineering and the Frontiers Science Center for Smart High-speed Railway System, Beijing Jiaotong University, Beijing 100044, China, and also with the Henan High-Speed Railway Operation and Maintenance Engineering Research Center, Zhengzhou 451460, China (e-mail: myang@bjtu.edu.cn).

time to ensure reliable V2V and V2I communications.

To achieve the above goals, environment information must be acquired firstly, i.e. environment sensing. RGB images taken by cameras are widely used forms of visual sensing data that contain information about propagation environment due to convenience and low cost [18]. Secondly, features of key scatterers are extracted from original visual data based on CV. Finally, AI-based methods can be used to achieve channel prediction (such as received power prediction) through processed image.

A. Related Work

Classical methods have been widely used in channel prediction. Narrowband and wideband channel measurements are carried out in [19]–[21] and [22]–[24], respectively. Channel characteristics such as path loss (PL), delay spread, angle spread etc. are extracted, modeled and analyzed based on measured data. Refs. [25], [26] use ray tracing to virtually reconstruct real propagation scenario, and precisely simulates propagation law of each multipath component to achieve accurate characterization of channel. Furthermore, a pervasive channel modeling theory is pioneered in [27] and a 6G pervasive geometry-based stochastic model (GBSM) is then proposed, which for the first time can model channel characteristics of all frequency bands and all scenarios including mmWave and V2V channels. The statistical properties of proposed 6G pervasive GBSM are fully investigated in [28], providing interesting relationships of model parameters, statistic properties, frequency bands, and scenarios. The above classical methods usually rely on complex measurement data or high computational costs, and they fail to consider accuracy, complexity and utilization of environment information of at the same time.

The development of CV technology provides a powerful means for processing visual data, enabling vision-aided wireless communications to be implemented in a variety of application scenarios. Refs. [29]–[31] obtain simulated time series RGB images from base station and use recurrent neural networks (RNN) and convolutional neural networks (CNN) respectively to implement beam prediction, blocking prediction and proactive handoff in mmWave MIMO networks. Refs. [32], [33] have proposed novel mechanisms for predicting time series of received power and blockage prediction by using convolutional long short-term memory with depth images. Refs. [34]–[36] respectively use vision-aided methods with RGB images to achieve beam alignment in mmWave vehicle communications, multi-user matching and resource allocation, as well as ultra-reliable and low-latency communications in smart factory scenarios. Refs. [37]–[39] put forward different concepts of environment semantic to reduce redundancy of images and efficiently achieve beam and blockage prediction better in mmWave MIMO networks. It can be seen that these studies all focus on solving problems such as beam prediction and selection, blockage prediction, etc.. However, they are not applied to channel prediction to assist vehicular communications.

To sum up, this work is rarely mentioned in existing research, which is to realize accurate and efficient channel

prediction based on environment information extraction using vision-aided methods in vehicular communications. It will be helpful to promote further deep integration of AI and communication and also provide a set of solutions for realization of intelligent deployment and application of vehicular communication system.

B. Contributions

To address the issues discussed above, we presented some preliminary experimental results in our previous work of [1]. In this paper, a two-stage deep learning model for channel prediction is proposed for mmWave vehicular communications. Three mature CV methods and two widely used deep neural networks, i.e. YOLOv8 and ResNets, are combined. We believe that this is an interesting application that we can accurately predict channel characteristics, such as received power, using only environment RGB images. The main contributions of this paper are summarized as follows.

- A two-stage channel prediction model for mmWave V2I scenarios based on deep learning is proposed, and detailed steps for training the model using RGB images and wireless channel data are described.
- To accurately predict received power using only RGB images, three typical CV methods are presented to extract environment information, which are adding bounding box, binary mask and instance segmentation to scatterers of interest in original images respectively.
- Extensive experiments are carried out based on open source measurement datasets, comparison of predictive performance of models with different processed images and with or without interference elimination are used as input, generalization of trained model on datasets in different scenarios and conditions, impact of different neural network scales on model prediction accuracy all have been discussed in detail. Results has validated the excellent performance of proposed model in practicability, reliability, and generalization.

The remainder of this paper is organized as follows. Section II describes the framework of two-stage model based on DL proposed in this paper. Section III introduces experiment setup and acquisition, selection and utilizability of datasets. Then in Section IV, a series of experiments about performance validation and analysis for proposed model is presented. Finally, Section V draws the conclusions.

II. VISION-AID CHANNEL PREDICTION MODEL

A. System Model

In this study, we consider a typical V2I communication scenario, where a base station (BS) is located at an intersection along the roadside, as shown in Fig. 1. Furthermore, BS is equipped with a transmitting antenna and a standard-resolution RGB wide-angle camera, which together enable communication and environmental monitoring. The mobile user (i.e., target vehicle) is equipped with a receiving antenna capable of receiving vector channel sounding signals transmitted by

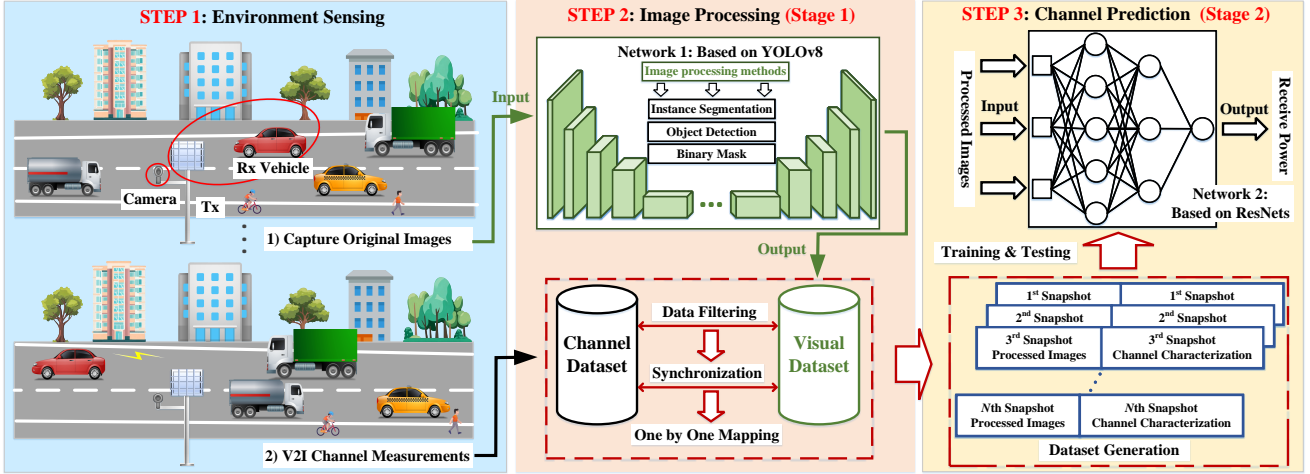


Fig. 1. Framework of proposed two-stage channel prediction model.

BS. Without considering MIMO, channel impulse response $h(t, \tau)$ can be expressed as [40]

$$h(t, \tau) = \sum_{l=1}^L \alpha_l e^{-j\phi_l} \delta(t - \tau_l), \quad (1)$$

where t is index of time snapshot, L are the number of rays, and τ_l is the delay of the L -th path. What's more, $\delta(\cdot)$ is the Dirac delta function, and ϕ_l is the phase of paths that is assumed to be described by statistically independent random variables uniformly distributed over $[0, 2\pi)$. Performing Fourier transform on $h(t, \tau)$ can obtain the channel transfer function $H(f)$. Thus we can obtain channel characteristics, typical examples of which include PL, delay spread τ_{rms} , received power P , etc.

B. Problem Formulation

The task of channel prediction is to capture the evolving trends of channel in order to inform key aspects of communication systems, such as network planning, base station placement, power control, etc. Traditional approaches typically rely on channel models, statistical methods based on channel measurements, or deterministic methods such as ray tracing and parabolic equations, to predict channel propagation characteristics. However, channel models established based on traditional methods often struggle to balance accuracy with computational complexity, lack generalization and adaptability across diverse scenarios, and fail to leverage the characteristics of propagation environment.

A promising alternative is the application of AI, particularly CV, to perceive propagation environment and thereby assisting in channel prediction. Visual data, which can be easily acquired and does not consume valuable spectrum resources, represents a valuable out-of-band resource. In recent years, research on exploring the use of visual data to assist wireless communication has gained traction, particularly in areas such as blockage prediction, beamforming prediction, and proactive handoff in mmWave networks. In this paper, we propose the use of additional visual data—specifically, RGB images

captured by camera installed on BS conjunction with CV and deep learning to predict channel. Notely, instead of using raw images, we follow the suggestion of [37] and use RGB images processed by different CV methods.

Formally, we define $X[t] \in \mathbb{R}^{W \times H \times C}$ as the corresponding RGB image at time t , where W , H , C are the width, height, and the number of color channels of the image. Let, $Z[t]$ represent processed RGB images. The objective of channel prediction task in this paper is to find a mapping function f_{Θ} that utilizes $Z[t]$ to predict channel characteristics $\hat{c}[t] \in \Omega$, $\Omega = [PL, \tau_{rms}, P...]$. The mapping function can be formally expressed as

$$f_{\Theta} : Z[t] \rightarrow \hat{c}[t]. \quad (2)$$

In this paper, we develop a deep learning model to learn this prediction function h_{Θ} . Let $D = \{(Z_m, c_m^*)\}_m^M$ represent available dataset consisting of “processed RGB image-channel characteristic” pairs is collected from wireless propagation environment as shown in Fig. 1, where M is the total number of snapshots in the dataset. In addition, loss function can be expressed as

$$L = \frac{1}{M} \sum_{m=1}^M \zeta(c_m^*, \hat{c}_m), \quad (3)$$

where $\zeta(\cdot)$ is the loss of a single snapshot, which measures the difference between predicted value and actual value. Then, the goal is to minimize the loss over all snapshots in the dataset D , which can be formally written as

$$f_{\Theta^*}^* = \arg \min_{f_{\Theta}} L(c_m^* | Z_m, \hat{c}_m). \quad (4)$$

The prediction function is parameterized by a set of model parameters Θ and is learned from the labeled data in the dataset D . The objective is to find the best parameters Θ^* that minimize the loss function. Next, we present the proposed vision based solution for channel prediction.

C. Framework

In this paper, we present a vision-aided two-stage deep learning model to predict channel characteristics, especially

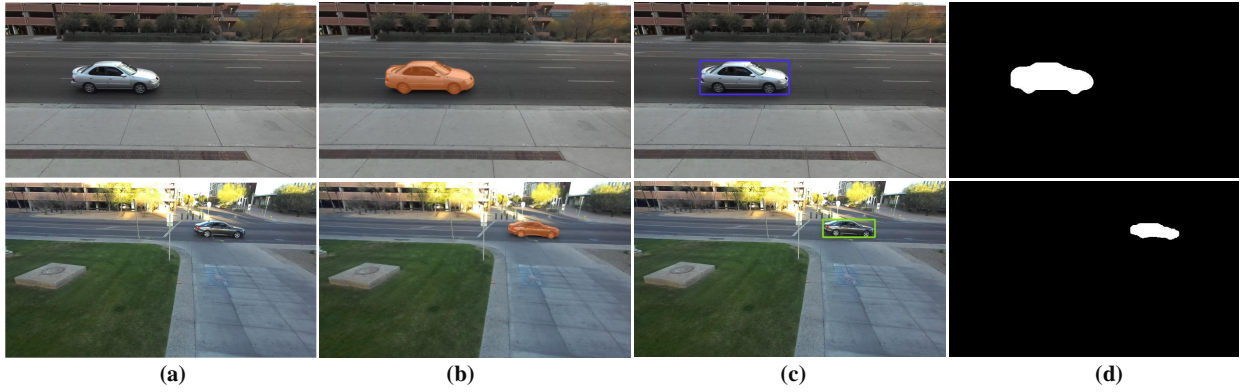


Fig. 2. Examples of three kind of images based on different CV methods. (a) Original images; (b) Images with instance segmentation; (c) Images with object detection; (d) Images with binary mask.

using received power as a study case. Framework of the model is shown in Fig. 1, which can be divided into three steps: environment sensing, image processing and channel prediction. The complete implementation is described in detail below.

Step 1: Environment Sensing. In this step, two independent datasets need to be collected. First, the camera mounted on BS (or roadside infrastructure) continuously captures RGB images of propagation environment, forming a original image dataset. Second, V2I channel measurements are conducted in the same environment to obtain vector channel data, which constitutes a channel dataset.

Step 2: Image processing. Image processing involves explicitly labeling target vehicle in the original images using various CV techniques as shown in Fig. 2, which includes object recognition with rectangular bounding boxes, instance segmentation with color masks, or segmentation using black-and-white masks. This facilitates the prediction network in Step 3 by enabling it to more effectively learn image features, thereby improving the accuracy of received power predictions. In Fig. 2(b), Outline of target vehicle is covered by pixels of the same color, and other scatterers remain unchanged. In Fig. 2(c), we use object detection to frame target vehicle with a rectangular frame, and other scatterers also remain unchanged. Entire image is covered by a binary mask in Fig. 2(d), in which target vehicle is filled with white pixels, while others are completely filled with black pixels. The impact of three types of images on prediction accuracy will be discussed in detail in Section IV.

In Step 2, original image dataset is firstly fed into Network 1, and processed images are generated to form visual dataset. The next critical step is to filter and synchronize channel data with processed visual data to establish a complete one-to-one mapping. This is essential because not all raw data obtained can be directly utilized for training and testing. Redundant data, such as images where target vehicle is absent, or visual and channel data that cannot be synchronized by timestamps due to inconsistent acquisition rates, offer limited value for training prediction network in Step 3.

It should be mentioned that Network 1 in Step 2 we have used is YOLOv8. YOLOv8 [41] is used to implement

extraction of environment information in this paper. YOLOv8 is released by Ultralytics company in 2023, which has shown significant improvements in accuracy and speed compared with previous versions [42]. More importantly, YOLOv8 has the functions of object detection, instance segmentation and binary mask addition. And pre-trained models provided by Ultralytics company after training on COCO dataset [43] are also available. It provides great convenience for extracting environmental information based on transfer learning.

Step 3: Channel Prediction. Processed images are fed into Network 2 to output predicted values of channel characteristics in Step 3, and we take received power as an example. Residual neural network (ResNet) has been widely used in CV tasks and has excellent ability to deal with both classification and regression problems. Therefore, ResNets proposed in [44] with various network scales are adopted and customized to fit received power prediction problem, including ResNet-18, ResNet-34, ResNet-50, ResNet-101 and ResNet-152. ResNets we use have been pre-trained on ImageNet2012 dataset [45], and network structure of them are the same as in [44], except for their final fully connected layers, which are removed and replaced with another fully connected layers of one output. This is because received power prediction is a regression task and final output is unique power value in dBm. ResNets are then fine-tuned, in a supervised fashion, using images from environment that are labeled with corresponding received power. The performance in different scenarios and impact of different network scales on prediction accuracy will be discussed in detail in Section IV.

III. EXPERIMENTAL SETUP

A. Datasets acquisition

The data used in this paper are from well-known open source dataset *DeepSense 6G* [46]–[48]. *DeepSense 6G* is a real-world multi-modal dataset designed to facilitate the development of sensing-aided wireless communication applications [49]. In this paper, only datasets of RGB images and received power have been used and they are derived from Scenarios 1-4 and 8-9 in *DeepSense 6G*, which are obtained from three different streets (named street 1, street 2 and street 3). It should be noted that Scenarios 1, 2 and 3, 4 represent both day and

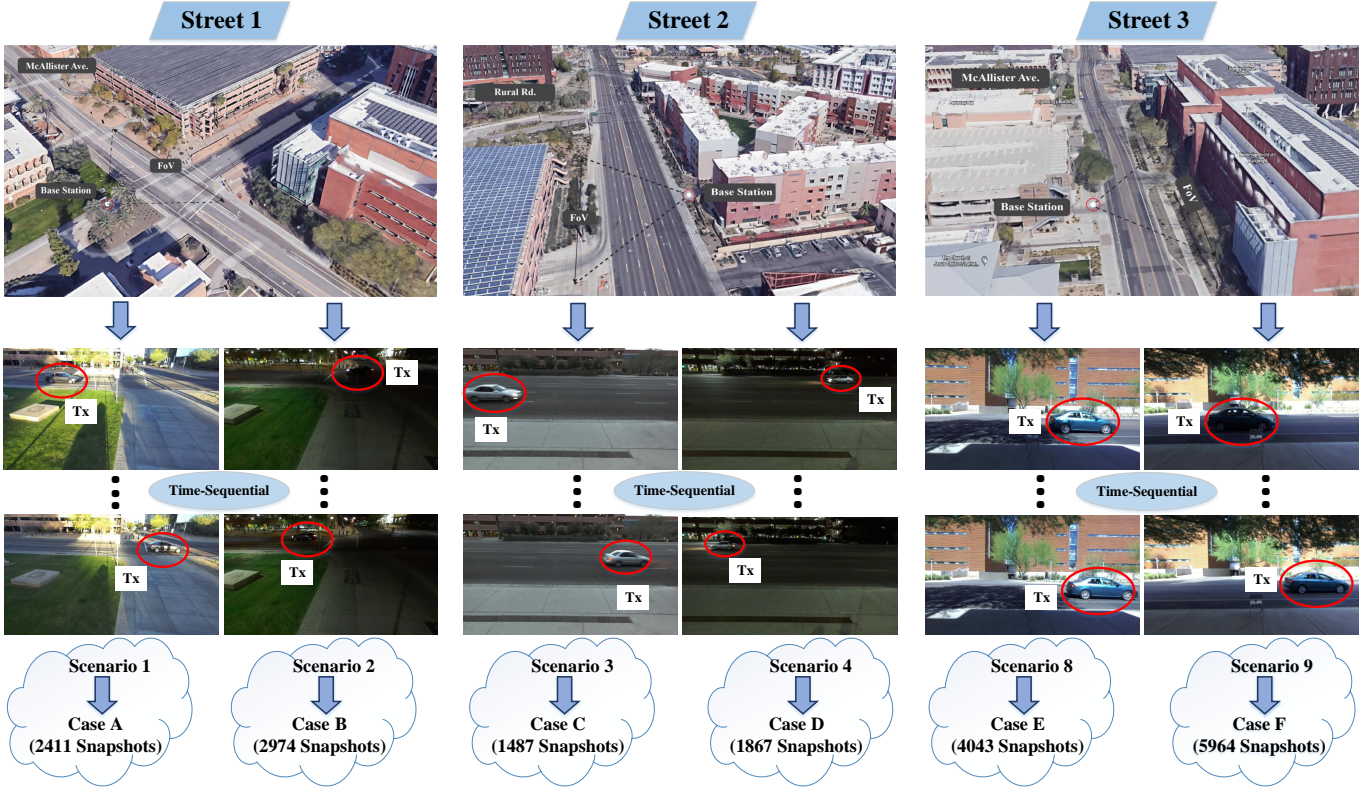


Fig. 3. Measurement scenarios for different streets and different situations (day or night).

night conditions on streets 1 and 2, respectively, and Scenarios 8 and 9 represent only day conditions on street 3, as shown in Fig. 3. For more convenient description, we will rename above six scenarios as Cases A, B, C, D, E and F.

The above six scenarios are selected because: 1) They are all typical V2I mmWave communication scenarios; 2) the street trend in collected images is relative smooth and gentle, almost parallel to camera's angle of view; 3) measurement system is the same for all cases, including configurations of antennas, cameras, etc.. In addition, they also have certain differences. For example, distance between base station (i.e. Rx) and different streets is not exactly the same, which results in different sizes of Tx vehicles in images despite the same viewing angle; color and size of Tx vehicles on three streets are different, and more importantly, there will be random non-test vehicles and pedestrians on each street, which may cause non-line-of-sight (NLOS) conditions and affect radio propagation. They are also recorded by RGB camera and further influence prediction accuracy of model.

The measurement system consists of transmitter (Tx) and receiver (Rx) [46]. Rx includes mmWave receiver, a 60 GHz RF front-end with a 16-element uniform linear array (SIVERS semiconductors), and an RGB camera with 110° field-of-view (FoV) and 30 frames per second (ZED2 from StereoLabs). Tx employs a mmWave transmitter with a 60 GHz quasi-omni antenna (SIVERS semiconductors). During measurement process, Rx is fixed, while Tx is installed on a vehicle and moves back and forth along fixed route in two-lane streets. During this period, Rx continuously obtains received power

TABLE I
CONFIGURATION OF MEASUREMENT SYSTEM.

Parameters	Description
Center Frequency	60 GHz
Transmitter antenna	Omni-directional antenna
Receiver antenna	16-Element antenna array
Average sample rate	8 Snapshots/s
Resolution of original images	960×540
Frame rate of camera	30 Frames per second
FoV of camera	110°
Average speed of vehicle	40 km/h

from Tx and captures RGB images. Detailed parameters of measurement system are shown in Table I.

B. Data Preprocessing

Data in dataset *DeepSense 6G* has been cleaned and pre-processed [46]. Through methods such as data synchronization, filtering and verification, it is ensured that data of received power corresponds to RGB images, which meets our experiment requirements, so we basically make no additional change to the original dataset. However, it should be pointed out that since our main task is to predict received power through RGB images, in order to simplify calculation amount, although mmWave receiver is a 16-element antenna array, we

TABLE II
HYPERPARAMETERS OF PROPOSED TWO-STAGE MODEL.

Hyperparameters	Description
Network for Stage 1	YOLOv8
Network for Stage 2	ResNets
Image size as input	224×224 pixels
Number of training epochs	50
Batch size	64
Loss function	MSE
Optimization algorithm	Adam
Activation function	ReLU
Learning rate	0.001

only use data of one certain channel. An overview of datasets for training and validation is shown in Fig. 3.

It should be noted that in datasets we use, there are line-of-sight (LOS) conditions between Tx vehicle and Rx with 90% probability, and at least 75% of time there is only a Tx vehicle exists in captured images and no other disturbing objects, such as non-test vehicles and pedestrians. This is reasonable, because in the wide-angle FoV of camera, unless it is a highly congested road section, occlusion between vehicles is not obvious, which creates conditions for LOS propagation. What's more, whether there are disturbing objects and whether to identify them in captured images have a huge impact on prediction accuracy and speed of model, which will be discussed in detail in Section IV-E.

It also should be explained that since datasets from *DeepSense 6G* uses only received power to describe wireless channel, prediction of channel characteristics in this work is also limited to received power. However, prediction of received power is still meaningful and important for vehicular communications. For example, if visual data obtained from base station can be used to help predict user's received power, it would be able to provide real-time guidance for base station power control and link budget without taking up additional spectrum, time and space resources, which will greatly improve the safe and efficient operation of vehicular communications. What's more, it is still important to emphasize that this study focuses on cross-field application innovation rather than focusing on specific channel parameters. It is foreseeable that since received power can be predicted, PL, delay spread and even Rice K-factor can actually be predicted as long as dataset is appropriate.

C. Model Training

Datasets we use contain received power and RGB images data of multiple streets as mentioned before, which are divided into training, validation and test sets in different proportions in various experiments. Specific dataset division is listed in Table III and introduced in Section IV. Original RGB images labeled with corresponding received power are used to train two-stage model. Resolutions of all input images on model training and validation is $960 \times 540 \times 3$ pixels (three

colour channels, RGB), and resolutions of images with BBox, instance segmentation and binary mask obtained by YOLOv8 are $960 \times 540 \times 3$, $960 \times 540 \times 3$ and $640 \times 384 \times 1$ pixels, respectively, and then they are all resized to 224×224 pixels to match input size of ResNets. It should be noted that both YOLOv8 and ResNets have been pre-trained on COCO dataset and ImageNet2012 dataset by transfer learning, respectively, and pre-trained weights have been fine-tuned on training sets. Through transfer learning (i.e., using a pre-trained existing network architecture), we can achieve good prediction performance even with a limited dataset. What's more, it is not to be ignored that categories of dynamic scatterers are only vehicles (including Tx vehicle and non-test vehicles) and pedestrians in selected image datasets, and they are all included in COCO dataset, thus pre-trained and fine-tuned YOLOv8 can almost accurately identify above dynamic scatterers.

Hyperparameters of YOLOv8 can be referred to [42]. And hyperparameters of prediction model in stage 2 are shown in Table II. Number of training epochs and batch size are 50 and 64 respectively, with learning rate 0.001. Adam [50] is selected as optimization algorithm and mean square error (MSE) function, which is widely used for regression tasks, is selected as loss function, with activation function of ReLU. Both YOLOv8 and ResNets are trained using deep learning framework PyTorch.

IV. PERFORMANCE EVALUATION AND ANALYSIS

Based on *DeepSense 6G*, we carry out a series of experiments to fully evaluate and analyze the performance of proposed two-stage model on received power prediction. Root mean square error (RMSE) is chosen as metric to evaluate prediction accuracy of model.

A. Experiment 1: Scenario Self-Validation

The purpose of this experiment is to verify prediction performance of model on different test sets after being trained on training sets from the same scenarios as test sets. In this experiment, we select four sets of data, cases A, C, E and F, representing day conditions of streets 1, 2 and 3, respectively. For division of datasets, first we randomly divided data of each case into training set and test set according to the proportion of 90% and 10%. Then we mix training sets of four cases together and randomly divided them into training and validation sets in proportions of 80% and 10% of total data. Finally, We get training, validation and test sets which account for 80%, 10% and 10% of total data respectively, in which test set contains independent data from four cases.

Taking case A as example, prediction results are shown in Fig. 4. RMSEs of received power prediction in four cases from three streets when different images are used are shown in Fig. 5(a). It should be noted that three types of images are used to predict received power respectively, thus in fact, these are three sub-experiments. Division of datasets in each sub-experiment is random, so test sets of three sub-experiments are not identical. Therefore, ground truths are not the same in subfigures in Fig. 4. For case A, RMSEs of BBox, segmentation and binary mask as inputs to prediction networks

TABLE III
CONFIGURATION OF FIVE EXPERIMENTS.

Experiments	Training and Validation Set	Test Set	Numbers of Total/Training/Test Data	Train/Validate/Test Dataset Ratio	Prediction Network
Scenario Self-Validation	Cases A, C, E and F (Day on Streets 1/2/3)		13905 / 12515 / 1390	80% / 10% / 10%	ResNet18
Day/Night Cross-Validation	Cases A, C, E and F (Day on Streets 1/2/3)	Cases B and D (Night on Streets 1/2)	18746 / 13905 / 4841	(Cross Validation)	ResNet-18
Scenario Cross-Validation	Cases A, B, C and D (Day and Night on Streets 1/2)	Case F (Day on Street 3)	14703 / 8739 / 5964	(Cross Validation)	ResNet-18
Impact of Network Scales	Cases A, C, E and F (Day on Streets 1/2/3)	Case A (Day on Street 1)	13905 / 11494 / 2411	85% / 10% / 5%	ResNet-18 ResNet-34 ResNet-50 ResNet-101 ResNet-152
Impact of Interference Elimination	Cases C and D (Day and Night on Street 2)		3354 / 3019 / 335	80% / 10% / 10%	ResNet-34

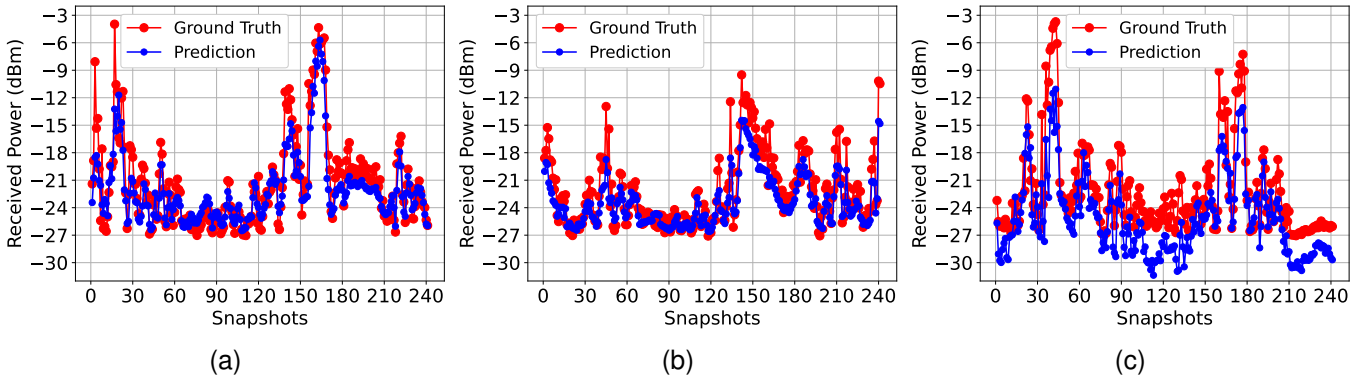


Fig. 4. Prediction results of three kinds of images in Experiment 1. Case A of Street 1: (a) BBox; (b) Instance Segmentation; (c) Binary Mask.

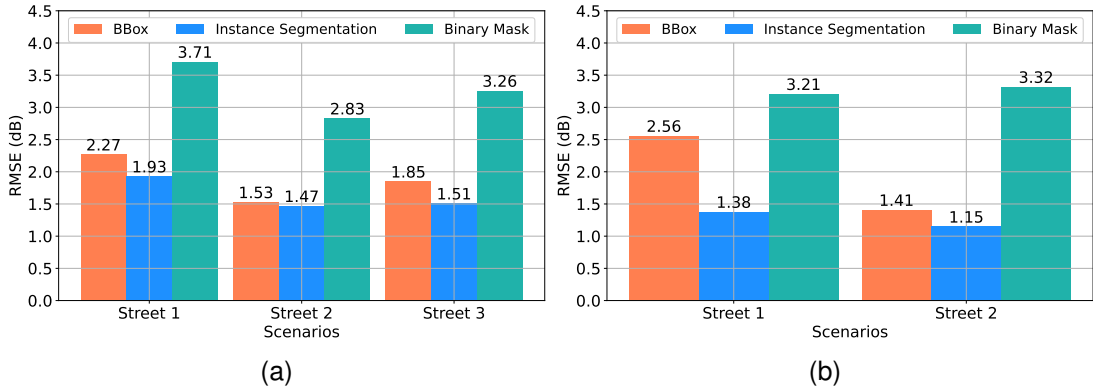


Fig. 5. RMSEs of prediction in (a) : Experiment 1: Scenario Self-Validation and (b) Experiment 2: Day/Night Cross-Validation.

are 2.27, 1.93 and 3.71 dB, respectively. For streets 2 (Case C) and 3 (Cases E and F), RMSEs are 1.53, 1.47, 2.83 and 1.85, 1.51, 3.26 dB, respectively. It can be found that received power prediction of three types of images is relatively accurate, and RMSEs are no more than 4 dB, which indicates that received power can be predicted accurately. What's more, it is interesting to note that images with instance segmentation has the smallest error, while images with binary mask has

the worst result. We suspect that this may be because the former not only highlights dynamic scatterers, but also retains static scatterers. Therefore, networks can learn features of environment more fully, while the latter does not contain complete static scatterers and only dynamic scatterers have been highlighted through white pixels. Networks do not learn environment features from images deeply enough, resulting in larger errors. While images with BBox retain static scatterers,

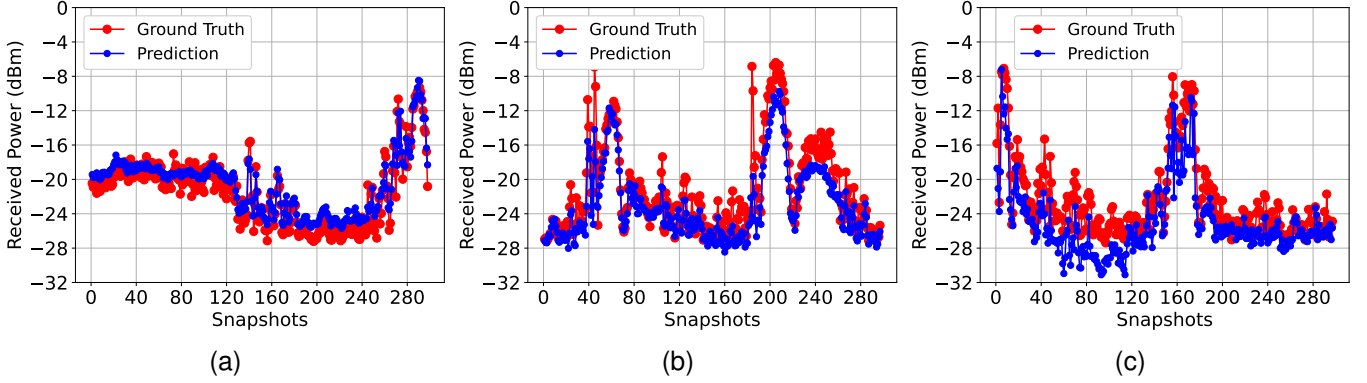


Fig. 6. Prediction results of three kinds of images in Experiment 2. Case B of Street 1: (a) BBox; (b) Instance Segmentation; (c) Binary Mask.

but prominence of dynamic scatterers is slightly inferior to that of instance segmentation, thus prediction performance is in the middle.

B. Experiment 2: Day/Night Cross-Validation

For RGB camera, it can more accurately capture environmental information during the day due to abundant light, while light at night will be darker, and description of environment in RGB images will be more blurred. Therefore, in this cross-validation experiment, we try to use the data under day conditions to train model, and take data under night conditions from the same street as test sets to validate generalization of proposed model. Cases A, C, E and F from day situations of streets 1, 2, 3, are used as training sets, while cases B and D representing day situations of streets 1 and 2 are selected as test sets.

RMSEs of prediction with different segmentation images are shown in Fig. 5(b), and prediction results on case B are shown in Fig. 6. To present results clearly and visually, only 10% of data in case B has been randomly captured and placed in Fig. 6. For street 1 (Case B), RMSEs of images with BBox, instance segmentation and binary mask are 2.56, 1.38, and 3.21 dB, respectively, and for street 2 (Case D), RMSEs are 1.41, 1.15, 3.32 dB. It can be seen that although prediction network in stage 2 is trained on datasets of day conditions, when RGB images at night have been input, model also can accurately predict received power.

We can find that similar to Experiment 1, when images with instance segmentation are used as input, prediction accuracy is the highest, while images with binary mask have the worst accuracy. Reasons for this phenomenon are same as Experiment 1. What's more, an interesting point is that for prediction network in stage 2 trained on the same dataset, no matter whether images in test sets are from day or night, network can achieve excellent received power prediction, and their prediction accuracy is not much different. On the one hand, it is due to powerful image processing capability of prediction network. On the other hand, this may be due to the fact that in addition to large differences in pixel colors between images from day and night, both static and dynamic scatterers in images captured are highly similar. What's more, artificial

light sources such as street lamps and vehicle lights are available at night in urban scenarios, which reduces the difficulty of network's recognition of scatterers, and further facilitates prediction network's learning of environment features, so that prediction accuracy of model for day and night images is not subject to wide-scale fluctuations.

C. Experiment 3: Scenario Cross-Validation

The purpose is to verify generalization ability of trained model on test sets from new scenarios in this experiment. Cases A, B, C, D are selected as training set from day and night of streets 1 and 2, respectively, and cases E, F from street 3 during the day are selected as test set.

Similarly, we still use three types of images to evaluate performance. Prediction results of BBox, instance segmentation and binary mask have been shown in Fig. 7 and their RMSEs are 4.46, 3.42 and 3.76 dB, respectively, only 200 snapshots are included in the figure for ease of observation. It can be seen that three networks can still roughly predict the trend of received power, but compared with Experiments 1 and 2, prediction accuracy is somewhat decreased. Prediction error on images with instance segmentation is still the smallest, while images with BBox is the largest, and their RMSEs are increased by 2-3 dB. However, RMSE of images with binary mask basically does not change, which indicates that images from new scenarios has little impact on prediction network trained on images with binary mask. This is due to characteristics of binary mask itself, in which only dynamic scatterers are additionally displayed with white areas, while static environment is covered by black areas, thus scenario changes are not actually visible in images with binary mask. What's more, it should be noted that decline in prediction performance of above three networks may also come from differences between data sets. In Figs. 4 and 6, values of received power fluctuates between -30 dB and 0 dB, while in Fig. 7, the value varies from -50 dB to -20 dB, and prediction networks are trained on data of the former and tested on the latter. The inconsistencies between received power ranges in training and test sets lead to degradation of prediction performance.

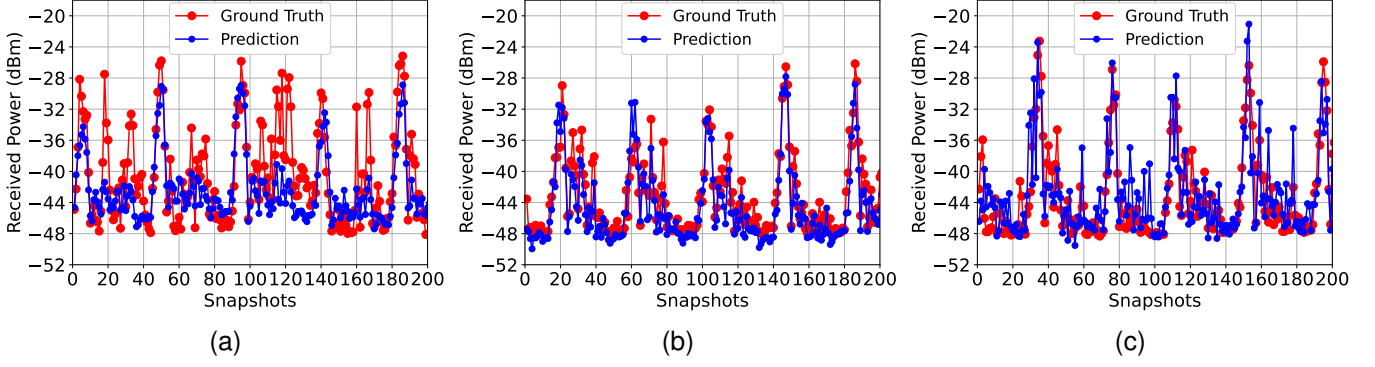


Fig. 7. Prediction results of three kinds of images in Experiment 3. (a) BBox; (b) Instance Segmentation; (c) Binary Mask.

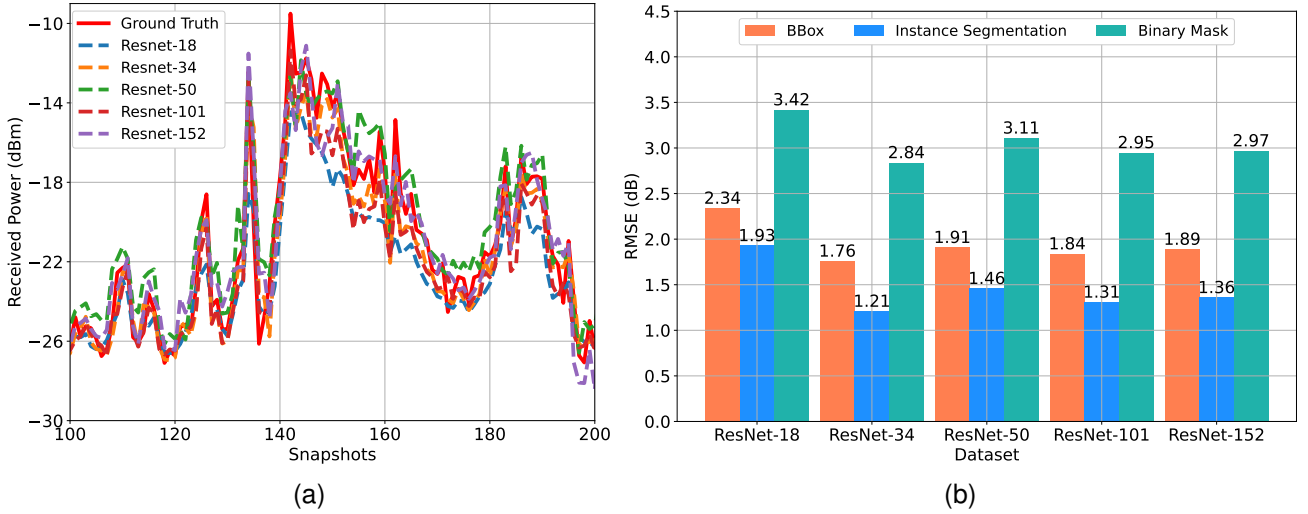


Fig. 8. Prediction results of images with instance segmentation and RMSEs of different CNNs with three types images in Experiment 4. (a) Prediction results of images with instance segmentation; (b) RMSEs of different CNNs with three types images.

D. Experiment 4: Impact of Network Scales

In fact, network in stage 1 is only responsible for converting original RGB images into images with environment, which does not directly affect prediction accuracy of model, because YOLOv8 after pre-trained and fine-tuned can almost achieve all of image conversion, and network in stage 2 really affects prediction accuracy of the whole model. In the first three experiments, we have used Resnet-18, which achieves relatively accurate prediction results. In this experiment, we try to use different layers of ResNets as prediction networks to validate impact of network scales on model performance. Networks we choose include ResNet-18, ResNet-34, ResNet-50, ResNet-101 and ResNet-152, with network depths of 18, 34, 50, 101 and 152 layers, respectively. Datasets of cases A, C, E and F are still selected, and divided methods of datasets are similar to Experiment 1, except that test set this time only comes from case A, day condition on street 1. We randomly selected 30% of data in case A as test set, with a total of 723 sets of data, accounting for about 5% of total data volume. The other training and validation sets are based on total data volume, divided into 85% and 10%.

Results of received power prediction using images with

instance segmentation as an example and RMSEs of different CNNs with three types images in this experiment are shown in Fig. 8. To present results clearly, only 100 snapshots in test set are shown in Fig. 8(a). As can be seen from Fig. 8(a), ResNets with different scales have better predictive effects on received power and can predict trend of received power. Even so, it also can be found that RMSEs of different CNNs still have gaps. Among them, ResNet-34 has the smallest RMSEs, the second is ResNet-50, followed by ResNet-151 and 152, they are very close, while the largest RMSEs are from ResNet-18. It can be seen that in the case of three types of images being input to predict received power, with the deepening of CNNs, prediction performance will be improved, but when a certain threshold is reached, if network scale continues to deepen, it will not only bring additional computing costs, but also obtain fairly small benefits. For ResNet-151 and ResNet-152, their networks differ by 51 layers, but RMSE only increases by 0.02-0.05 dB. However, decreasing network scale will also lead to poorer performance, thus reasonable trade-off is necessary.

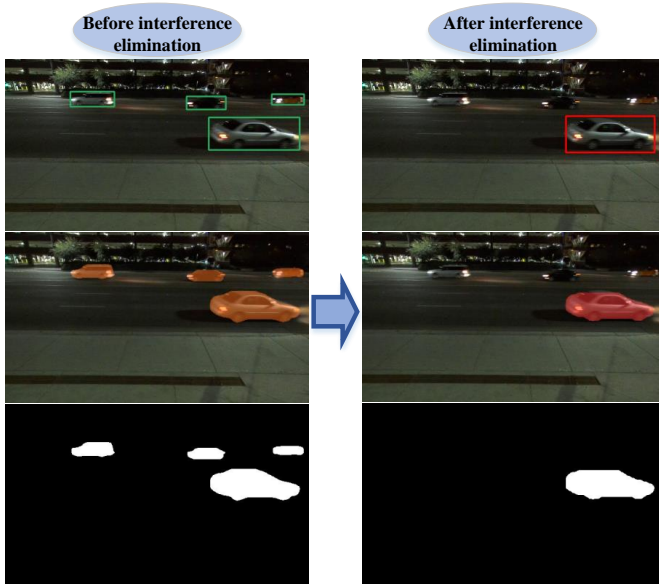


Fig. 9. Image comparison before and after interference elimination.

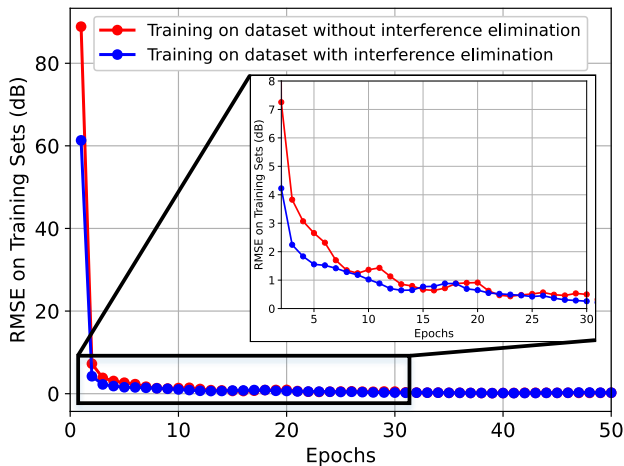


Fig. 10. RMSEs on different training sets in Experiment 5.

E. Experiment 5: Impact of Interference Elimination

Three types of image highlight features of each dynamic scatterer in previous four experiments, including Tx vehicle, non-test vehicles and pedestrians, while YOLOv8 do not accurately identify Tx vehicle and only highlight it. In this experiment, we generate images in which only Tx vehicle is highlighted, while other non-test dynamic scatterers are no longer highlighted like static scatterers, which called interference elimination. Then we use these images to train prediction network to validate prediction performance of model after interference elimination.

To achieve above purpose, we need to retrain YOLOv8 and we have to manually label original RGB images. Datasets we selected are cases C and D, representing both day and night conditions of street 2, with a total of 3522 data. First, we use tool Labelme [51] to draw rectangular boxes around Tx vehicle in order to generate BBox, and then using software X-Anylabelling [52] to outline Tx vehicle in order to generate

segmentation and binary mask. In fact, we only manually label about 2000 images and use them to train YOLOv8, and remaining approximately 1500 images are automatically generated by YOLOv8 after training. Through above steps, we obtain images of only Tx vehicle highlighted, as shown in Fig. 9. We have randomly divided them into training, validation and test sets according to ratio of 80%, 10% and 10%, without distinguishing day and night conditions. In stage 2, we choose Resnet-34 as prediction network because it has been proved to have the best performance in Experiment 4.

Results of received prediction using images with instance segmentation as an example and RMSEs of two conditions with three types images in this experiment are shown in Figs. 11(a) and (b). Only 100 snapshots in test set are shown in Fig. 11(a) for ease of observation. It can be seen that prediction network trained using images after interference elimination has better performance. RMSEs on images with BBox, instance segmentation and binary mask are 0.78, 0.68 and 0.94 dB, respectively, and RMSEs of with images before interference elimination are 1.45, 1.19 and 2.13 dB, respectively. Fig. 10 demonstrates RMSEs of each epoch when model is trained on datasets with and without interference elimination. It can be found that model trained on both datasets converges at epoch 30 and interference elimination is more conducive to improving convergence speed and prediction accuracy of model. We can find that model has more powerful prediction performance when features of exclusive target object is labeled, while too many non-target objects are labeled, which brings burden to prediction network, resulting in a decline in prediction speed and accuracy of network.

F. Discussion

To adequately evaluate performance of model, we have conducted five experiments to verify it from different aspects. First, we verify prediction accuracy on test sets from different scenarios in Experiment 1, with RMSE arrange from 1.47 to 3.71 dB. Secondly, cross-validation has been used to verify generalization in Experiments 2 and 3. Networks trained using day data from the same street work well for night predictions, with RMSE between 1.15-3.32 dB. Although accuracy of prediction networks tested on new scenarios will decrease, trend of received power can still be predicted generally with RMSEs between 3.42-4.46 dB. Results of these two experiments prove that the proposed model has fairly good generalization. Then, effects of network scale in stage 2 on prediction accuracy have been discussed in Experiment 4. The results demonstrate that relationship between network scale and prediction accuracy is not linear, and reasonable tradeoffs are needed. Moreover, with moderate number of network layers and best prediction accuracy, Resnet-34 should be prioritized for channel prediction tasks. Finally, we analyze impacts of interference elimination on prediction results in stage 1 in Experiment 5. The results show that eliminating interference and keeping only features of target object will be more beneficial to prediction accuracy and efficiency of the model. Therefore, for V2I scenarios of single user, accurately identifying features of user will be more conducive to predict

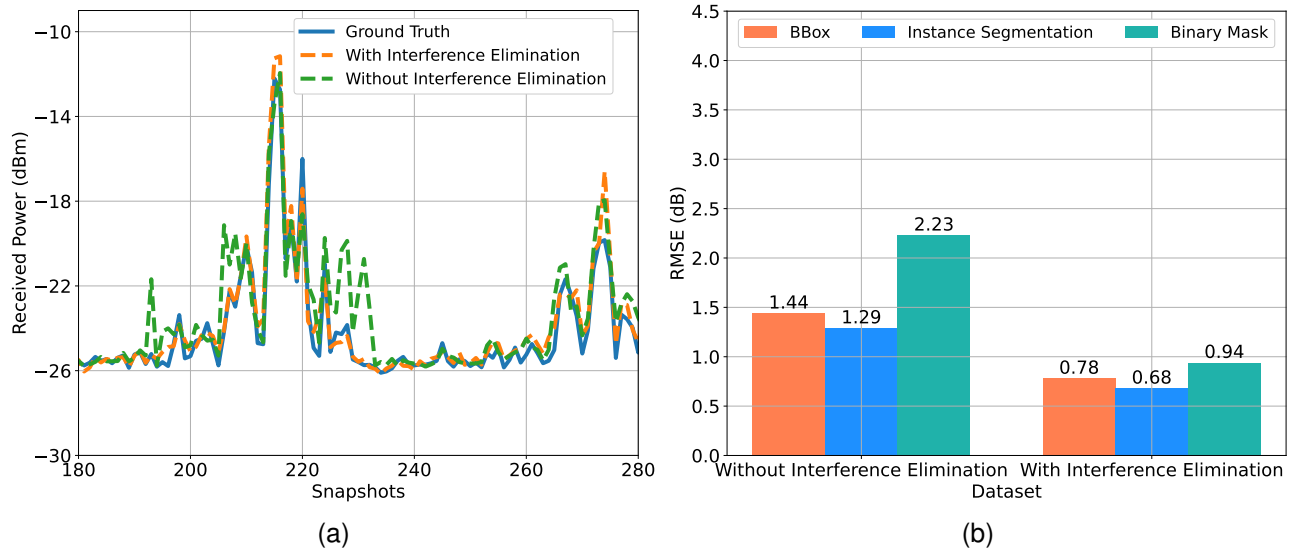


Fig. 11. Prediction results of images with instance segmentation and RMSEs of before/after interference elimination with three types images in Experiment 5. (a) Prediction results of images with instance segmentation; (b) RMSEs of before/after interference elimination with three types images.

wireless channel. Moreover, it should not be ignored that in all five experiments, highest prediction accuracy is achieved when images with instance segmentation are input in stage 2, while images with binary mask have the worst accuracy. Therefore, instance segmentation-based method will be more beneficial to received power prediction.

V. CONCLUSION

In this paper, vision-aided two-stage model based on CV for channel prediction in mmWave vehicular communication scenarios has been proposed. Firstly, original images about different propagation environment are obtained through RGB camera, and three methods of environment information extraction based on CV are applied. Secondly, a vision-aided two-stage channel prediction model has been established. Finally, five experiments are carried out based on measurement datasets to evaluate performance of the proposed model. Experiment results have validated the excellent performance in practicability, reliability and generalization. The model in this paper has the advantages of high accuracy, simple operation and high implementation efficiency. It is achieved by using only RGB images of propagation environment to predict received power of user. The ideas in this paper can be extended to prediction of other typical channel characteristics. It will be helpful to promote further deep integration of AI (especially CV) technology and wireless communication and also provide a set of novel solutions for realization of intelligent vehicular communication system.

REFERENCES

- [1] X. Zhang, R. He, M. Yang, Z. Zhang, Z. Qi, and B. Ai, "Vision-aided channel prediction with RGB images for mmwave communications," in *2024 IEEE International Symposium on Antennas and Propagation and INC/USNC-URSI Radio Science Meeting (AP-S/INC-USNC-URSI)*, 2024, pp. 1845–1846.
- [2] ITU-R, "Future technology trends of terrestrial International Mobile Telecommunications systems towards 2030 and beyond," *Report M.2516-0*, Nov. 2022. [Online]. Available: https://www.itu.int/dms_pub/itu-r/opb/rep/R-REP-M.2516-2022-PDF-E.pdf
- [3] ITU-R, "Framework and overall objectives of the future development of IMT for 2030 and beyond," *DRAFT NEW RECOMMENDATION*, Jun. 2023.
- [4] C. Huang *et al.*, "Artificial intelligence enabled radio propagation for communications—Part I: Channel characterization and antenna-channel optimization," *IEEE Trans. Antennas Propag.*, vol. 70, no. 6, pp. 3939–3954, 2022.
- [5] R. He, N. D. Cicco, B. Ai, M. Yang, Y. Miao, and M. Boban, "COST CA20120 INTERACT framework of artificial intelligence-based channel modeling," *IEEE Wirel. Commun.*, pp. 1–8, 2025.
- [6] A. Graff, Y. Chen, N. González-Prelcic, and T. Shimizu, "Deep learning-based link configuration for radar-aided multiuser mmwave vehicle-to-infrastructure communication," *IEEE Trans. Veh. Technol.*, vol. 72, no. 6, pp. 7454–7468, 2023.
- [7] Y. Zhang *et al.*, "Generative adversarial networks based digital twin channel modeling for intelligent communication networks," *China Commun.*, vol. 20, no. 8, pp. 32–43, 2023.
- [8] C. Huang *et al.*, "Artificial intelligence enabled radio propagation for communications—part II: Scenario identification and channel modeling," *IEEE Trans. Antennas Propag.*, vol. 70, no. 6, pp. 3955–3969, 2022.
- [9] Z. Qiu, R. He, M. Yang, S. Zhou, L. Yu, C. Wang, Y. Zhang, J. Fan, and B. Ai, "CNN-based path loss prediction with enhanced satellite images," *IEEE Antennas Wireless Propag. Lett.*, vol. 23, no. 1, pp. 189–193, 2024.
- [10] M. Yang, R. He, B. Ai, C. Huang, C. Wang, Y. Zhang, and Z. Zhong, "AI-enabled data-driven channel modeling for future communications," *IEEE Commun. Mag.*, pp. 1–7, 2023.
- [11] Z. Qi *et al.*, "Point cloud-based environment reconstruction and ray tracing simulations for railway tunnel channels," *High-speed Railway*, vol. 1, no. 4, pp. 241–247, 2023.
- [12] M. Yang *et al.*, "Machine-learning-based scenario identification using channel characteristics in intelligent vehicular communications," *IEEE Trans. Intell. Transp. Syst.*, vol. 22, no. 7, pp. 3961–3974, 2021.
- [13] Y. Tian, G. Pan, and M.-S. Alouini, "Applying deep-learning-based computer vision to wireless communications: Methodologies, opportunities, and challenges," *IEEE Open J. Commun. Society*, vol. 2, pp. 132–143, 2021.
- [14] T. Nishio, Y. Koda, J. Park, M. Bennis, and K. Doppler, "When wireless communications meet computer vision in beyond 5G," *IEEE Communications Standards Magazine*, vol. 5, no. 2, pp. 76–83, 2021.
- [15] R. He and Z. Ding, *Applications of machine learning in wireless communications*, 2019, vol. 81.
- [16] M. Yang *et al.*, "Dynamic V2V channel measurement and modeling at street intersection scenarios," *IEEE Trans. Antennas Propag.*, vol. 71, no. 5, pp. 4417–4432, May 2023.

- [17] R. He *et al.*, "Propagation channels of 5G millimeter-wave vehicle-to-vehicle communications: Recent advances and future challenges," *IEEE Veh. Technol. Mag.*, vol. 15, no. 1, pp. 16–26, 2020.
- [18] Y. Jin and D. Wang, "Study on static deflection model of MEMS capacitive microwave power sensors," *Chinese J Electron.*, vol. 33, no. 5, pp. 1188–1195, 2024.
- [19] X. Zhang, R. He, M. Yang, Z. Qi, Z. Zhang, B. Ai, and R. Chen, "Narrowband channel measurements and statistical characterization in subway tunnels at 1.8 and 5.8 GHz," *IEEE Trans. Veh. Technol.*, pp. 1–13, 2024.
- [20] X. Zhang *et al.*, "Measurements and modeling of large-scale channel characteristics in subway tunnels at 1.8 and 5.8 GHz," *IEEE Antennas Wireless Propag. Lett.*, vol. 22, no. 3, pp. 561–565, 2023.
- [21] R. He, Z. Zhong, B. Ai, J. Ding, Y. Yang, and A. F. Molisch, "Short-term fading behavior in high-speed railway cutting scenario: Measurements, analysis, and statistical models," *IEEE Trans. Antennas Propag.*, vol. 61, no. 4, pp. 2209–2222, 2013.
- [22] Z. Zhang, R. He, B. Ai, M. Yang, X. Zhang, R. Chen, H. Zhang, and Z. Zhong, "A shared multipath components evolution model for integrated sensing and communication channels," *IEEE Antennas Wireless Propag. Lett.*, vol. 22, no. 12, pp. 2975–2978, 2023.
- [23] Y. Zeng *et al.*, "Measurement and simulation for vehicle-to-infrastructure communications at 3.5 GHz for 5G," *Wirel. Commun. Mob. Comput.*, vol. 2020, pp. 1–13, Dec. 2020.
- [24] M. Yang *et al.*, "Measurements and cluster-based modeling of vehicle-to-vehicle channels with large vehicle obstructions," *IEEE Trans. Wireless Commun.*, vol. 19, no. 9, pp. 5860–5874, Sep. 2020.
- [25] Y. Wang, K. Venugopal, A. F. Molisch, and R. W. Heath, "MmWave vehicle-to-infrastructure communication: Analysis of urban microcellular networks," *IEEE Trans. Veh. Technol.*, vol. 67, no. 8, pp. 7086–7100, 2018.
- [26] L. Wang, B. Ai, D. He, K. Guan, J. Zhang, J. Kim, and Z. Zhong, "Vehicle-to-infrastructure channel characterization in urban environment at 28 GHz," *China Commun.*, vol. 16, no. 2, pp. 36–48, 2019.
- [27] C.-X. Wang, Z. Lv, X. Gao, X. You, Y. Hao, and H. Haas, "Pervasive wireless channel modeling theory and applications to 6G GBSMs for all frequency bands and all scenarios," *IEEE Trans. Veh. Technol.*, vol. 71, no. 9, pp. 9159–9173, 2022.
- [28] C.-X. Wang, Z. Lv, Y. Chen, and H. Haas, "A complete study of space-time-frequency statistical properties of the 6G pervasive channel model," *IEEE Trans. Commun.*, vol. 71, no. 12, pp. 7273–7287, 2023.
- [29] M. Alrabeiah, J. Booth, A. Hredzak, and A. Alkhateeb, "Viwi vision-aided mmwave beam tracking: Dataset, task, and baseline solutions," *arXiv preprint arXiv:2002.02445*, 2020.
- [30] M. Alrabeiah, A. Hredzak, and A. Alkhateeb, "Millimeter wave base stations with cameras: Vision-aided beam and blockage prediction," in *Proc. IEEE 91st Veh. Technol. Conf. (VTC-Spring)*, 2020, pp. 1–5.
- [31] G. Charan, M. Alrabeiah, and A. Alkhateeb, "Vision-aided 6G wireless communications: Blockage prediction and proactive handoff," *IEEE Trans. Veh. Technol.*, vol. 70, no. 10, pp. 10 193–10 208, 2021.
- [32] T. Nishio, H. Okamoto, K. Nakashima, Y. Koda, K. Yamamoto, M. Morikura, Y. Asai, and R. Miyatake, "Proactive received power prediction using machine learning and depth images for mmWave networks," *IEEE J. Sel. Areas Commun.*, vol. 37, no. 11, pp. 2413–2427, 2019.
- [33] Y. Koda, J. Park, M. Bennis, K. Yamamoto, T. Nishio, M. Morikura, and K. Nakashima, "Communication-efficient multimodal split learning for mmWave received power prediction," *IEEE Commun. Lett.*, vol. 24, no. 6, pp. 1284–1288, 2020.
- [34] W. Xu, F. Gao, Y. Zhang, C. Pan, and G. Liu, "Multi-user matching and resource allocation in vision aided communications," *IEEE Trans. Commun.*, vol. 71, no. 8, pp. 4528–4543, 2023.
- [35] W. Xu, F. Gao, X. Tao, J. Zhang, and A. Alkhateeb, "Computer vision aided mmwave beam alignment in V2X communications," *IEEE Trans. Wireless Commun.*, vol. 22, no. 4, pp. 2699–2714, 2023.
- [36] Y. Feng, F. Gao, X. Tao, S. Ma, and H. V. Poor, "Vision-aided ultra-reliable low-latency communications for smart factory," *IEEE Trans. Commun.*, pp. 1–1, 2024.
- [37] S. Imran, G. Charan, and A. Alkhateeb, "Environment semantic aided communication: A real world demonstration for beam prediction," in *Proc. IEEE Int. Conf. Commun. Workshops (ICC Workshops)*, 2023, pp. 48–53.
- [38] Y. Yang, F. Gao, X. Tao, G. Liu, and C. Pan, "Environment semantics aided wireless communications: A case study of mmWave beam prediction and blockage prediction," *IEEE J. Sel. Areas Commun.*, vol. 41, no. 7, pp. 2025–2040, 2023.
- [39] F. Wen, W. Xu, F. Gao, C. Pan, and G. Liu, "Vision aided environment semantics extraction and its application in mmWave beam selection," *IEEE Commun. Lett.*, vol. 27, no. 7, pp. 1894–1898, 2023.
- [40] Y. Ma *et al.*, "Orthogonal delay-doppler division multiplexing modulation with tomlinson-harashima precoding," *IEEE Trans. Commun.*, pp. 1–13, 2024.
- [41] G. Jocher, A. Chaurasia, and J. Qiu, "Ultralytics YOLO," Jan. 2023. [Online]. Available: <https://github.com/ultralytics/ultralytics>
- [42] F. M. Talaat and H. ZainEldin, "An improved fire detection approach based on YOLO-v8 for smart cities," *Neural Comput. Appl.*, vol. 35, no. 28, pp. 20 939–20 954, 2023.
- [43] T.-Y. Lin, M. Maire, S. Belongie, J. Hays, P. Perona, D. Ramanan, P. Dollár, and C. L. Zitnick, "Microsoft coco: Common objects in context," in *Proc. European Conf. Comput. Vis.*, 2014, pp. 740–755.
- [44] K. He, X. Zhang, S. Ren, and J. Sun, "Deep residual learning for image recognition," 2015.
- [45] O. Russakovsky *et al.*, "Imagenet large scale visual recognition challenge," *Int. J. Comput. Vis.*, vol. 115, pp. 211–252, 2015.
- [46] A. Alkhateeb, G. Charan, T. Osman, A. Hredzak, J. Morais, U. Demirhan, and N. Srinivas, "Deepsense 6G: A large-scale real-world multi-modal sensing and communication dataset," *IEEE Commun. Mag.*, vol. 61, no. 9, pp. 122–128, 2023.
- [47] G. Charan, T. Osman, A. Hredzak, N. Thawdar, and A. Alkhateeb, "Vision-position multi-modal beam prediction using real millimeter wave datasets," in *Proc. IEEE Wireless Commun. Netw. Conf. (WCNC)*, 2022, pp. 2727–2731.
- [48] A. Alkhateeb and G. Charan, "Computer vision aided blockage prediction in real-world millimeter wave deployments," in *Proc. IEEE Globecom Workshops (GC Wkshps)*, Rio de Janeiro, Brazil, Dec. 2022, pp. 1711–1716.
- [49] G. Charan and A. Alkhateeb, "User identification: A key enabler for multi-user vision-aided communications," *IEEE Open J. Commun. Society*, vol. 5, pp. 472–488, 2024.
- [50] D. P. Kingma and J. Ba, "Adam: A method for stochastic optimization," *arXiv preprint arXiv:1412.6980*, 2014.
- [51] K. Wada, "Labelme: Image Polygonal Annotation with Python." [Online]. Available: <https://github.com/wkentaro/labelme>
- [52] W. Wang, "Advanced auto labeling solution with added features," <https://github.com/CVHub520/X-AnyLabeling>, CVHub, 2023.